Clays and Clay Minerals, Vol. 68, No. 5:413–427, 2020

EFFECTS OF BIO-BASED PLASTICIZERS, MADE FROM STARCH, ON THE PROPERTIES OF FRESH AND HARDENED METAKAOLIN-GEOPOLYMER MORTAR: BASIC INVESTIGATIONS

Adrian Tutal *, Stephan Partschefeld, Jens Schneider, and Andrea Osburg

[1]Faculty of Civil Engineering, F. A. Finger-Institute for Building Materials Engineering, Chair of Building Chemistry and Polymer Materials, Bauhaus-Universität Weimar, Weimar, Germany

Abstract—Conventional superplasticizers based on polycarboxylate ether (PCE) show an intolerance to clay minerals due to intercalation of their polyethylene glycol (PEG) side chains into the interlayers of the clay mineral. An intolerance to very basic media is also known. This makes PCE an unsuitable choice as a superplasticizer for geopolymers. Bio-based superplasticizers derived from starch showed comparable effects to PCE in a cementitious system. The aim of the present study was to determine if starch superplasticizers (SSPs) could be a suitable additive for geopolymers by carrying out basic investigations with respect to slump, hardening, compressive and flexural strength, shrinkage, and porosity. Four SSPs were synthesized, differing in charge polarity and specific charge density. Two conventional PCE superplasticizers, differing in terms of molecular structure, were also included in this study. The results revealed that SSPs improved the slump of a metakaolin-based geopolymer (MK-geopolymer) mortar while the PCE investigated showed no improvement. The impact of superplasticizers on early hardening (up to 72 h) was negligible. Less linear shrinkage over the course of 56 days was seen for all samples in comparison with the reference. Compressive strengths of SSP specimens tested after 7 and 28 days of curing were comparable to the reference, while PCE led to a decline. The SSPs had a small impact on porosity with a shift to the formation of more gel pores while PCE caused an increase in porosity. Throughout this research, SSPs were identified as promising superplasticizers for MK-geopolymer mortar and concrete.

Keywords—Bio-based · Geopolymer · Metakaolin · Starch · Superplasticizer

INTRODUCTION

Used at a rate of ~4 Gt/a, cement is the most widely deployed binding agent in construction materials (Andrew). In spite of constant improvements in the energy efficiency of manufacturing processes over recent decades and the increasing substitution of cement clinker by materials such as ground granulated blast-furnace slag (GGBS), fly ash (FA), and metakaolin (MK), cement production is responsible for the emission of ~1.5 Gt/a of CO_2. This corresponds to ~4% of the annual global anthropogenic CO_2 emissions (Le Quéré 2018).

Cement-substitute materials such as GGBS, FA, and MK have a glassy alumosilicate structure and also react with alkaline activators (alkali hydroxide solution or alkali silicate solution) to form an aluminosilicate network (ASN). In highly alkaline environments, the X-ray amorphous aluminosilicates dissolve and condense to an ASN and transform further to a zeolite-like structure in which the activator is incorporated (Davidovits 2005).

These binders, known as alkali activated binders (AAB) or geopolymers, show partly improved properties in comparison to ordinary Portland cement (OPC) and have been researched intensively, most notably during the past decade. Thus, greater early strengths (Fernández-Jiménez and Palomo 2007), better resistance to attack by organic acids (Koenig et al. 2017) and sulfates (Elyamany 2018), and improved fire resistance (Saxena et al. 2017) at temperatures of up to 800°C (Kuenzel et al. 2013) as well as smaller CO_2 emissions during production (Turner and Collins2013) have been observed.

Unlike GGBS and FA, MK is produced from natural resources and is independent of technological advances and industrial migration, which aim to achieve local availability and lower cost. MK is obtained by dehydroxylation of kaolin at temperatures of between 450 and 1000°C. CaO may be present due to impurities in the raw materials or additives but the amount is much less than found in either GGBS or FA. The BET surface area of MK can exceed 15 m^2/g but increases the water demand, which does not favor the use of MK geopolymers as binders in mortars and concretes.

The influence of the initial water content on MK-geopolymer mortar was investigated by Pouhet et al. (Pouhet et al. 2019) who found that with increasing water content the compressive strength decreased linearly, while the porosity increased proportionally. More than 90 wt.% of the added water was unbound and evaporated while drying at 105°C. Compared to OPC-derived mortar, a much greater permeability for air and chloride ions was found.

The influence of water content and chemical composition on the structural properties of ambient cured MK-geopolymers was studied by Lizcano et al. (2012). The study showed that most of the water contained in the specimens evaporated within the first 7 days and then the evaporation rate dropped significantly. After 21

* E-mail address of corresponding author: adrian.tutal@uni-weimar.de

DOI: 10.1007/s42860-020-00084-8

days, comparable water contents, independent of the initial ratio of $H_2O/(Al_2O_3 + SiO_2)$, were determined. Na-activated samples contained larger amounts (15–20 wt.%) of unevaporated water compared to K-activated samples (6–10 wt.%), however. After 145 days, no significant further loss of water was observed compared to day 21. With increasing $H_2O/(Al_2O_3 + SiO_2)$ ratio, an increase in open porosity and a decrease in bulk density were observed.

Gharzouni et al. (2016) found that besides the water content, the reactivities of the metakaolin and the alkaline activator have an influence on the porosity. With increasing reactivity of the components, a reduced porosity with growing average pore size was observed, which was associated with an increased nucleation and the formation of smaller particles causing a denser structure.

Superplasticizers are used to reduce the water content of a mixture while maintaining its workability. In conventional cementitious mortars and concretes, high-performance superplasticizers made of polycarboxylate ethers (PCE) are used widely. Generally, PCE consist of a main chain (trunk chain) of poly-methacrylic acid and many side chains (graft chains) along that main chain. Two different PCE types of side chain can be distinguished. The simplest type of PCE is the MPEG-PCE in which methoxy polyethylene glycol (PEG) side chains are distributed randomly along the main chain. A comprehensive overview of the various types of PCE was given by Plank et al. (2015). Calcined clays, despite their X-ray amorphous structure, have residual aluminosilicate layers resulting originally from the clay structure. Superplasticizers based on MPEG-PCE are sensitive to clay minerals because the polyethylene glycol side chains intercalate into the interstitial layers of the clay minerals. Due to this chemisorption, the steric effect of the PCE is disabled. In addition, physisorption in the form of electrostatic attraction between the cationic-charged surface of the clay minerals and the anionic main chain occurs. The cationic charge is caused by Ca^{2+} cations from the cementitious pore solution being adsorbed onto the surface of the clay minerals. With greater grafting density of the PCE as well as with a larger dosage, intercalation is dominant over the surface adsorption. Adsorption of PCE on clay minerals is up to 100 times greater in comparison to cement (Ng and Plank 2012). These results imply an extraordinary consumption of PCE leading to an unfavorable foaming effect. Conventional PCE showed the greatest decline in dispersing ability while montmorillonite was present in the cement. Smaller declines in dispersing ability were found for kaolin, followed by muscovite. A PCE free of polyethylene glycol (PEG) showed only a minor decline in dispersing ability even if exposed to montmorillonite (Lei and Plank 2014). Newly developed PCE on the basis of methacrylic acid hydroxyalkyl methacrylate (MAA-HAMA) with very short side chains possess good clay tolerance in cementitious systems (Lei and Plank 2012). This new type of PCE shows a strongly decreased adsorption tendency on clay minerals, which could cause difficulties if applied to pure clay systems. No specific plasticizing product for alkaline activated binders is currently available on the market.

The influence of basic media on different superplasticizers was investigated by Palacios and Puertas (Palacios and Puertas 2004). Using Fourier-transform infrared (FTIR) spectroscopy, FT-Raman, and ultraviolet-visible (UV-Vis) spectroscopy, most of the superplasticizers studied showed structural changes at pH > 13. However, the naphthalene- and polypropylene-glycol-based superplasticizers proved to be stable in a sodium hydroxide solution (pH 13.6), whereas only the latter was also stable in sodium silicate solution. For example, a separation of the analyzed polycarboxylate-based superplasticizer's side chains from its main chains due to saponification/hydrolysis of the esters was found.

Comparative investigations were carried out by Favier et al. (2014) into the rheological behavior of a MK-geopolymer in contrast to an OPC-paste. The typical identifiable rheological behavior of an OPC-paste was shear thinning at shear rates in the low two-digit range. Colloidal interactions due to electrostatic and Van der Waals forces were decisive factors influencing the viscosity. At shear rates of ~100 r/min, the viscosity of the pore solution may outweigh these forces. Ultimately, at shear rates >>100 r/min, increasing collision and friction forces between the particles led to a shear-thickening behavior of the paste. On the other hand, the MK-geopolymer showed that viscous forces independent of the shear rates predominated and led to a viscosity curve that was scarcely dependent on the shear rate. Colloidal interactions were detected in the early phase of reactions with low intensity, which were obtained due to gel formation occurring during the hardening process. In summary, Favier et al. (2014) stated that the viscosity of the alkaline activator and the packing density of the metakaolin particles influenced the rheology significantly.

The bio-based starch superplasticizers (SSPs) derived from manioc starch, wheat starch, and starch from potato processing waste were synthesized by Partschefeld and Osburg (Partschefeld and Osburg 2018a, 2018b). The SSPs were synthesized in two steps. First, the molecular weight of the starch was reduced by acid hydrolysis with HCl. Then, the modification of starch molecules took place in an alkaline environment by sulfoethylation with sodium vinyl sulfonate. The effects of the SSPs on the viscosity of a cement paste were comparable to the effects of polycarboxylate ether (PCE) and polycondensate (PC) superplasticizers at the same dosage of plasticizer. The SSPs also led to a prolonged dormant period of the cement paste, which made an application for ready-mix concrete conceivable.

In recent decades, many studies have been conducted into the potential use of natural polymers as a superplasticizer in concrete. A comprehensive overview was given by Bezerra (2016). Generally, the most chain-like polymers show a plasticizing behavior when the chain length and the charge are adapted to the colloidal system. The influence of molecular weight and functional groups of cellulose ethers on the plasticizing properties of concrete were investigated by Knaus and Bauer-Heim (2003). Degraded and anionic, modified chitosan were demonstrated by Lv (2016) to work well over the long term compared to PCE and naphthalene sulfonate. According to Crépy et al. (2014), only sulfonated starch with a dosage of >1% resulted in a significant plasticizing effect on Portland cement concrete.

While other solutions for geopolymer systems exist, e.g. in the form of superplasticizers based on naphthalene sulfonate, SSPs have an ecological advantage because they can be derived from renewable sources as well as from industrial waste. The aim of the present study was to determine if SSPs are potentially suitable superplasticizers for MK-geopolymers through observation of the effects on the physical and mechanical properties of fresh and hardened mortar samples.

MATERIALS AND METHODS

Metakaolin

Metakaolin Metaver R (Newchem AG, Pfaffikon, Switzerland) was used as the mineral precursor material. The BET surface area of the material, 16 m^2/g, was determined using nitrogen in the relative pressure (P/P_0) range 0.05–0.2. The chemical analysis of the MK material was carried out by inductively coupled plasma-optical emission spectroscopy (Aktiva M, Horiba, France) (Table 1). Quantitative X-ray diffraction (XRD) analysis was carried out using a Seifert XRD 3003 TT diffractometer (GE Inspection Technology, Hamburg, Germany). The quantitative phase composition was calculated by Rietveld refinement (*AutoQuan* 2.0, XRD Eigenmann GmbH, Karlsruhe, Germany) using 10 wt.% zinc oxide as an internal standard. The sample, already containing the internal standard, was mixed with 2-propanol before milling and homogenization for 1 min in a McCrone Micronizing Mill (McCrone Scientific Ltd, London, UK) using corundum grinding bodies. The 2-propanol was evaporated by heating the sample to 40°C for 3 h. The sample was then front-loaded into the XRD. The step size was 0.03°2θ within an angle range of 4–70°2θ. The tube voltage and integration time per step were set to 40 kV and 5 s, respectively.

The results of the quantitative Rietveld analysis showed that the material consisted of 50.8 wt.% amorphous phases (Table 2). Obviously, half of the binder material contained metakaolin and the other half consisted of fines, including quartz, calcite, and anatase. The calcite content was comparable to the CaO content determined by chemical analysis. Thus, the reactive fraction consisted of 22.6% alumina and 28% silica.

Table 1. Results of chemical analysis of Metaver R

Oxide	Content (wt.%)
SiO_2	66.7
Al_2O_3	21.1
Fe_2O_3	4.6
CaO	2.1
MgO	0.4
TiO_2	1.03
MnO	0.01
K_2O	0.44
Na_2O	0.06
SO_3	0.0
$CaO_{(free)}$	< 0.1

Table 2. Results of XRD analysis of Metaver R

Phase	Content (wt.%)
Amorphous	50.8 ± 1.7
Quartz	44.7 ± 1.4
Calcite	3.0 ± 0.6
Anatase	1.6 ± 0.4

Because of the mostly inert states that abstain from geopolymer formation, whether crystalline phases can be considered as part of the binder is debatable. In common cementitious binder systems, limestone is found widely as an inert filler but is considered to be part of the binder. The amorphous as well as crystalline phases of Metaver R were considered to be part of the binder in the present study.

While less amorphous phases lead to a less dense structure, the large water demand of binders, due to the large specific surface area of metakaolin, can be reduced. A smaller amount of water leads to a smaller volume fraction of capillary pores, which are considered to be detrimental to durability.

Alkaline Activator

Betol K 57 M (Wöllner GmbH, Ludwigshafen, Germany), a potassium silicate solution, was used as the alkaline activator. The product had a total solid content of ~50 wt.%, determined by loss on ignition at 950°C. The mass fraction of silicon oxide was determined gravimetrically by applying soda borax digestion, while all other relevant mass fractions were calculated using hydrofluoric acid digestion. The calculated water glass module (SiO_2/K_2O ratio) was 1.1 and the pH was 14.

Fine Aggregate

Aggregate according to CEN standard EN 196-1:2016 was used as a fine aggregate. It is a quartz sand with a grain size of 0.08–2.00 mm. The sand was available in 1350 g containers.

Starch Superplasticizers (SSPs)

Four SSPs were synthesized from CrystalTEX626 (Ingredion Germany GmbH, Hamburg, Germany), a starch made from cassava plant roots, also called tapioca. The molecular weight of the pre-manufactured starch already fulfilled the requirements of the synthesis product. Therefore, no acid hydrolysis was necessary.

The synthesis took place in a heated container under constant stirring. The starch was mixed with deionized water at a ratio of 1:40. The solution was alkalized with NaOH-pellets (Carl Roth GmbH + Co. KG, Karlsruhe, Germany) and heated to 80°C. After reaching the target temperature, either sodium vinyl sulfonate (Sigma-Aldrich, Inc., Darmstadt, Germany) was added (in two steps) to introduce anionic charge or (3-chloro-2-hydroxypropyl) trimethylammonium chloride (Sigma-Aldrich, Inc., Darmstadt, Germany) was added to introduce cationic charge. With increasing reaction time, the specific charge density of the starch molecules increased. The reaction was carried out over two time periods, 24 h and 72 h, while maintaining a temperature of 80°C.

In total, four types of SSPs were synthesized: two flow agents with anionic charge (Fig. 1) and two flow agents with cationic charge (Fig. 2). The SSPs of the same charge polarity differed from each other by their specific charge density. Low charge density (LC) was achieved by reacting for 24 h after application of the synthesis reagents, high-charge density (HC) by reacting for 72 h. The naming scheme used for the SSPs consisted of a prefix 'S' and the abbreviations for the specific charge density (LC/HC) and the polarity (+/–). Uncharged SSPs were not part of the study because they had shown no beneficial impact on the viscosity of geopolymer paste in prior investigations which showed comparable similarities to the behavior of cementitious pastes analyzed by Partschefeld and Osburg (2018a, 2018b).

The specific charge density was determined using a particle charge detector (Mütek PCD-04, BTG Instruments GmbH, Wessling, Germany) equipped with a titration unit (Table 3). The SSPs with anionic charge differed from each other with respect to the specific charge density by a factor of >20. The SSPs with cationic charge varied by a factor of <2.

The molecular weight distribution of the base starch CrystalTex626 and the four synthesized SSPs were analyzed by gel permeation chromatography (JASCO Deutschland GmbH, Pfungstadt, Germany).

The number average and weight average molar mass as well as the polydispersity of the starch and the four starch-based SSPs were used to describe the molecular weight distribution (Table 4). The values described the distribution of count and weight of the (modified) starch molecules. The polydispersity described the relation between the number average and weight average molar mass and increased with a widening gap between the values. A small polydispersity was an indicator of a narrow molecular weight distribution.

The number average molar masses of the SSPs were 28–54% smaller than those of the base starch with the sample SHC– (54% smaller) deviating from the other samples (28–36% smaller). The values of SLC+ and SHC+ samples appeared to have small deviations from each other, while the values of SLC– and SHC– samples demonstrated a clear decrease in the number average molar mass with the specific surface charge and the reaction time. With the exception of the SLC– sample, the weight average molar mass of the other samples decreased by 37–58% compared to the base starch. Again, the values of SLC+ and SHC+ samples occurred with almost no deviations from each other. The SHC– and SLC– samples revealed a 37% smaller and

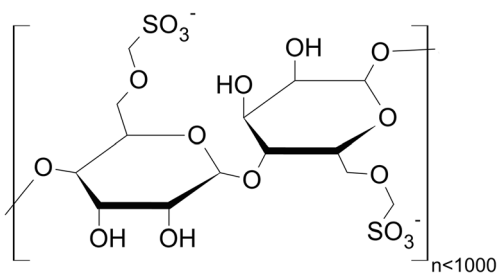

Fig. 1. Starch modified with sodium sulfonate

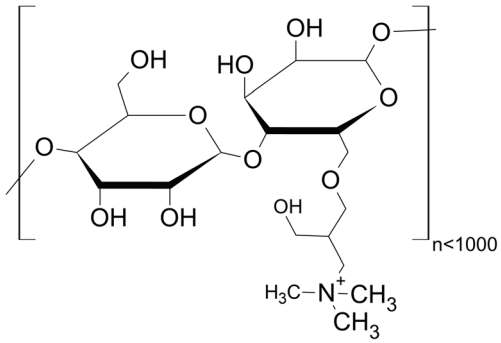

Fig. 2. Starch modified with CHPTAC

46% larger weight average molar mass, respectively, compared to the base starch.

The differences in number average and weight average molar mass are reflected in the degree of polydispersity, D_c. The SLC+ and SHC+ samples had very similar molecular weight distributions (Fig. 3). The degree of polydispersity of both samples was very similar, therefore, with values of 2.31 and 2.45, which are significantly <4, representing the degree of polydispersity of the base starch. As a result, the width of the molecular weight distribution decreased during the reaction. The samples SLC– and SHC–, on the other hand, showed clear differences with respect to the molecular weight distribution. The first and simultaneously highest peak of both samples revealed a larger value for SHC–, of which the number average molar mass was obtained as 1.71×10^3 g/mol. The number average molar mass of the sample SLC– with a value of 2.38×10^3 g/mol was located in the second peak. This peak was the same height for both samples. While sample SHC– showed a uniformly decreasing molar mass distribution with increasing molar mass after the third peak, sample SLC– indicated a clear increase. This was further emphasized by the comparatively large weight average molar mass of ~21.68×10^3 g/mol, while sample SHC– had a value of 9.21×10^3 g/mol. The difference in the molecular weight distribution of the SLC– and SLC+ samples was reflected in a clear deviation of the degree of polydispersity of both samples of 5.38 and 9.11, respectively. The values for samples SLC+ and SHC+ (Fig. 3) showed that the specimens with cationic charge had a narrower molecular weight distribution than their counterparts with anionic charge.

Table 3. Specific charge density of synthesized SSPs

	Specific charge density	
	(μEq/g) *	(C/g)
SLC–	32.9[a]	3.18
SHC–	786.4[a]	75.88
SLC+	101.2[b]	9.76
SHC+	182.1[b]	17.57

[a] Titrant: 0.001 N polydiallyldimethylammonium chloride (Poly-DADMAC)

[b] Titrant: 0.001 N sodium polyethylene sulfonic acid (PES-Na)

*(cmol(+)/kg) = (μeq/g)×0.1 (Reganold and Harsh1985)

Table 4. Weight and number average molar mass and polydispersity

	Number average molar mass *M*n (g/mol)[a]	Weight average molar mass M_w (g/mol)	Polydispersity D_c
CrystalTEX 626	3.73×10^3	1.48×10^4	3.98
SHC+	2.68×10^3	6.19×10^3	2.31
SLC+	2.59×10^3	6.34×10^3	2.45
SHC–	1.71×10^3	9.21×10^3	5.38
SLC–	2.38×10^3	21.68×10^3	9.11

[a] Determined by size exclusion chromatography with a pu-980 pump and separating columns NOVEMA3000 and NOVEMA300, DMSO/LiBr-solvent at 65°C

The Na^+ and Cl^- concentrations of the SSPs were calculated from the information given in the datasheets provided by the manufacturer. SSPs with anionic charge had a Na^+ concentration of 0.344 mol/L while SSPs with cationic charge contained a Na^+ and Cl^- concentration of 0.156 mol/L and 0.312 mol/L, respectively.

Polycarboxylate ether (PCE) superplasticizers

Two PCE superplasticizers (PCE1 and PCE2) with known structures were used to compare with the SSPs. These materials were produced by radical polymerization (Giovanni Bozzetto S.p.A., Filago, Italy). Both superplasticizers contained a defoamer which was dosed with 0.5 wt.% based on the solids content. Sowoidnich (2015) carried out a structural analysis of the superplasticizers providing information on the number of monomers of the main chain (N), the number of monomers of the side chains (P), and the repeating structural units (n) of the PCE. Based on these values, the PCE were assigned to a structure type of comb-like homopolymers (Gay and Raphaël 2001). PCE1 can be classified as a flexible backbone worm (FBW) polymer. These polymers are flexible due to long main chains as well as short side chains. While the main chains consist of methacrylic acid, the side chains consist of 23 polyethylene glycol (PEG) units. PCE1 had a molecular weight of 10.93 g/mol. The molecular weight was determined by gel permeation chromatography. The solids contents of the superplasticizers were obtained by freeze-drying until consistency of mass was reached. The polymer content of PCE1 corresponded to 40 wt.%. The structure of PCE2, on the other hand, can be classified as flexible backbone star (FBS) polymers. Due to flexible and long side chains, these polymers adopt a star-shaped structure where the side chains are directed outward. While the manufacturing method and starting materials were the same as for PCE1, the number of PEG units of the side chains was determined to be 114. This corresponded to a molecular weight of 20.8 g/mol for the PCE2, which was found to be twice as high as the value of PCE1. The active substance content of 40 wt.% was similar to that of PCE1 (Sowoidnich 2015).

Mix Design

Geopolymer pastes and mortars were produced as part of the investigations. The pastes consisted of a 3:2 mass ratio of Metaver R to Betol K 57 M. Hereafter, the total amount of Metaver R and the solids content of an alkaline activator were considered to be the binder. The water quantity was considered to be the sum of water introduced through the alkaline activator and, in the case of mortars, added deionized water. The alkaline activator, Betol K 57 M, had a solids content of 50 wt.%. The water/binder ratio of the geopolymer pastes was 0.25,

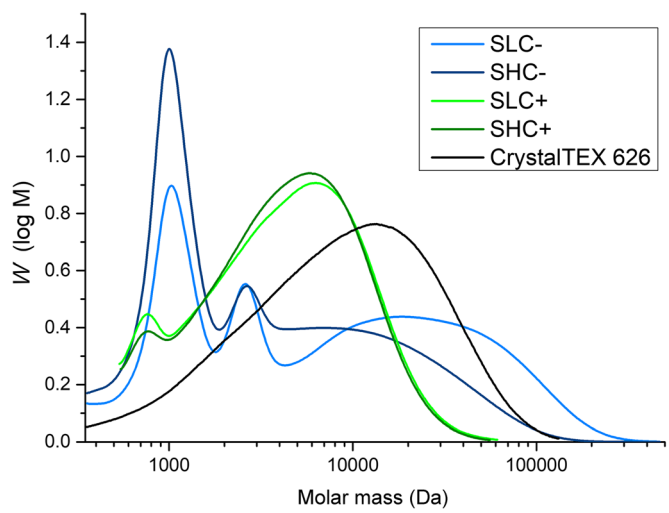

Fig. 3. SEC spectra of SSPs and base starch

Table 5. Mix design of reference paste and mortar

	Metaver R (g)	Betol K 57 M (g)	Water (g)	Sand (g)	Water/ Binder ratio
Paste	337.5	225	-	-	0.25
Mortar	337.5	225	112.5	1350	0.50

therefore (Table 5). The SiO_2/Al_2O_3 and Al_2O_3/K_2O ratios were ascertained to be 4.0 and 1.3, respectively.

The mortar mix designs were based on the reference mix design for cementitious mortars specified in EN 196-1:2016. The proportion of cement was replaced by the geopolymer paste described above. The amount of water introduced through the alkaline activator was counted toward the amount of water addition required in the standard. Sand as specified in EN 196-1:2016 was used as a fine aggregate. The binder-to-water-to-aggregate ratios of the geopolymer mortar were as 2:1:6 and, therefore, the water-to-binder ratio was determined as 0.5.

The dosage of superplasticizers added was based on the mass of superplasticizer solids and the amount of binder. Due to the application of superplasticizers in aqueous solution, the water content was counted towards the amount of mixing water to maintain a fixed water-to-binder ratio. Two dosages of superplasticizers were investigated: 0.5 and 1.0 wt.%.

Methods

The pastes and mortars were mixed using an electric stirrer. First, the metakaolin and alkaline activator were mixed together for 90 s to form a paste. In the case of the mortars, fine aggregate according to EN 196-1:2016 and deionized water were added and mixed with the paste for 90 s. The superplasticizer was added and mixed in the paste or mortar for another 90 s. In total, the mixing times amounted to 180 and 270 s for the pastes and mortar, respectively.

To characterize the fresh mortar, the slump, air content, and bulk density of two samples of each composition were determined. The slump measured according to EN 1015-3:1996 was viewed as a guideline value for workability and thus for the basic effectiveness of the superplasticizers. The bulk density and the air content were determined according to EN 1015-6:2006 and EN 1015-7:1998, respectively.

The influence of superplasticizers on the hardening of the mortars was investigated by ultrasonic running time using an Ultratest IP-8 (UltraTest GmbH, Achim, Germany) system. An ultrasonic pulse was introduced into the sample at intervals of 60 s over a period of 72 h. A detector was used to measure the ultrasonic time through the sample with a resolution of 0.05 μs. The ultrasonic velocity was then calculated from the ultrasonic time and the distance between the pulse transmitter and receiver. The analysis was carried out for two samples of each mortar composition.

The shrinkage behavior of the mortars containing 0.5 wt.% was investigated by a combined method of computer-controlled measurement in special shrinkage channels during the early phase of hardening and subsequent manual measurement of test specimens later on. During the computer-controlled examination, the shrinkage channels were sealed to be airtight so that only autogenous shrinkage could take place. After the specimens were removed from the shrinkage channels, the drying shrinkage was recorded by manual measurement at fixed intervals.

The shrinkage channels consisted of a formwork with the internal dimensions of 40 mm×40 mm×250 mm and a movable end surface with a displacement transducer. Measuring pins were screwed into both ends to enable a firm connection with the test specimen and to allow manual measurement later on. To minimize the frictional forces between the specimen and the formwork, the formwork was lined with two polypropylene films assembled on top of each along the bottom and sides. Before the formwork was filled, the movable end surface was fixed. The fixing was released after the sample started to solidify. The setting time for each sample had been determined previously.

The changes in length were recorded over a period of 72 h. The specimens were then removed from the formwork, measured and stored in ambient conditions (20°C/50% RH). Measurement of specimens was repeated at intervals of 7 days over a period of 28 days, then at intervals of 28 days. The tests were carried out on three test specimens per mortar.

To assess the influence of superplasticizers on the solid mortar properties, the flexural strength and compressive strength were determined according to EN 1015-11:1999 after 7 and after 28 days. Prisms of 40 mm×40 mm×160 mm were subjected to a three-point bending test until fracture. Then the compressive strength was determined on both fragments of the specimen. The flexural and compressive strengths were determined three times and six times, respectively. The strengths were obtained using TONI-Comp III (Toni Technik GmbH, Berlin, Germany) and TIRAtest 28100 (TIRA GmbH, Schalkau, Germany) instruments. Loading speeds were adjusted to 50 N/s for flexural strength and 2400 N/s for compressive strength.

The porosity of the freeze-dried mortar samples was investigated using mercury intrusion porosimetry at a sample age of 28 days. The AutoPore IV 9500 (Micromeritics GmbH, Unterschleißheim, Germany) was used to detect pores with pore radii from 0.003 to 245 μm at pressures of up to 206 MPa.

RESULTS AND DISCUSSION

Slump Tests

In comparison to the reference, which showed a slump of ~170 mm, the samples containing PCE1 and PCE2 achieved slump values reduced by as much as 5% (Fig. 4). This negative

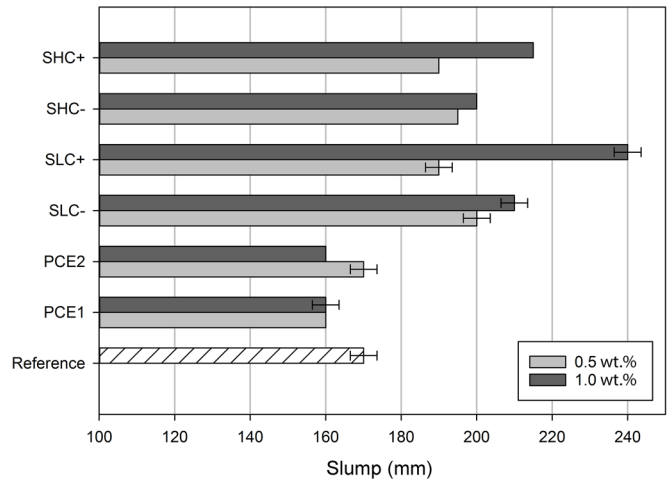

Fig. 4. Slump values of fresh mortars

effect increased with increasing dosage of PCE2. The samples containing SSPs showed slump values of up to 240 mm (SLC+). With the exception of the specimens containing SHC–, a clear increase in slump values of SSPs containing samples was observed with increased dosage.

At a dose of 0.5 wt.%, the samples containing SSPs reached slump values at between 190 and 195 mm, which corresponds to an increase of ~11–14%. At a dosage of 1.0 wt.%, the increase is 17–41%, which corresponds to slump values of 200–240 mm. While negatively charged SSPs led to slump values of between 195 and 210 mm, SSPs with positive charge resulted in values between 190 and 240 mm. The SSPs with positive charge appear to have had a stronger dispersion effect than the negatively charged SSPs, especially with increasing dosage of superplasticizer.

Both anionically and cationically charged SSPs showed a viscosity-reducing effect. Consequently, adsorption on particle surfaces is concluded for both species. While metakaolin is expected to have a negative surface charge, the small amount of Ca^{2+} ions introduced with the binder can lead to positive surface charges. Both types of SSPs can adsorb onto particle surfaces, therefore, and lead to (electro)-steric hindrance.

Air Content

All values of the air content were determined twice and rounded to a precision of 0.5 vol.% according to EN 1015-7:1998 (Table 6). The reference air content was 6.0 vol.%. Samples containing PCE-SP showed an increase in air content of up to 8.5 vol.% (PCE1) and 9.0 vol.% (PCE2).

Samples with SSPs revealed air contents of 5.5 vol.%, except samples containing high doses of SLC+ and SHC+ reached air contents of 6.0 vol.%.

Bulk Density

The bulk density of the fresh reference mortar was 2.21 g/cm^3 while all samples containing superplasticizers showed smaller bulk densities of between 2.05 and 2.15 g/cm^3 (Table 7). The smaller bulk density of the samples containing PCE1 or PCE2 corresponds well with the greater air content of the samples (Table 6). Because of the slightly smaller air content, the bulk densities of samples containing SSPs were expected to be equal to or greater than the bulk density of the reference specimen. The measured densities appeared to be smaller, however, and varied between 2.11 and 2.15 g/cm^3.

Ultrasonic-velocity Measurements

The results of the measurements (Fig. 5) of ultrasonic velocity on samples containing 1.0 wt.% of superplasticizer showed progressions that can be divided roughly into two groups. The reference, as well as most other samples, resulted in maximum ultrasonic velocities of between 18 and 24 h. The samples containing SLC–, SLC+, and PCE2 reached maximum ultrasonic velocities between 30 and 36 h, however. In addition to the changed behavior, the samples containing PCE2 also showed a lower maximum ultrasonic velocity than other samples. This can be traced back to the larger air content of the samples.

After reaching maximum ultrasonic velocity, the values decreased steadily by 700 m/s or 20% over the rest of the measurement period for all samples. This was attributed to water evaporation which occurred due to covering the samples

Table 6. Air content of fresh mortar

	Air content (vol.%)	
Reference	6.0 ± 0.0	
	0.5 wt.% SP dose	1.0 wt.% SP dose
PCE1	8.0 ± 0.0	8.5 ± 0.0
PCE2	9.0 ± 0.0	9.0 ± 0.0
SLC–	5.5 ± 0.0	5.5 ± 0.0
SHC–	5.5 ± 0.0	5.5 ± 0.0
SLC+	5.5 ± 0.0	6.0 ± 0.0
SHC+	5.5 ± 0.0	6.0 ± 0.0

Table 7. Bulk density of fresh mortar

	Bulk density (g/cm^3)	
Reference	2.21	
	0.5 wt.% SP dose	1.0 wt.% SP dose
PCE1	2.13	2.11
PCE2	2.07	2.06
SLC–	2.12	2.11
SHC–	2.12	2.13
SLC+	2.12	2.11
SHC+	2.15	2.15

with plastic caps inside the test chamber instead of using airtight lids. Only SSPs had a small impact on the hardening of MK-geopolymer mortar. Further research is needed to understand the processes involved in the slightly delayed hardening of samples containing SLC–, SLC+, and PCE2.

Shrinkage

Shrinkage behavior appeared to be similar for both dosages of PCE or SSPs with few deviations of ~0.05 mm/m (Figs 6 and 7).

Most samples shared the almost linear shrinkage behavior of the reference (Fig. 6). The linear shrinkage after 72 h for the reference reached ~0.1 mm/m. The smallest shrinkage, ~0.07 mm/m, was observed in samples containing SLC+. While samples with PCE1 led to linear shrinkage comparable to the reference, PCE2-containing samples showed much greater shrinkage in the timeframe of 6 to 68 h. This led finally to a linear shrinkage of ~0.36 mm/m after 68 h, with an expected further increase to 72 h. While SLC+-containing samples showed little shrinkage, the opposite can be seen for samples with SHC+. Larger shrinkage compared to the reference was obtained consistently, with an evenly increased shrinkage rate after 36 h. After 68 h a linear shrinkage of ~0.26 mm/m was reached.

After 72 h, the specimens were removed from the formwork and stored at ambient conditions. Measured shrinkage over a course of 58 days showed less shrinkage of all specimens in comparison to the reference (Fig. 7). Most shrinkage appeared to occur in the first 4 days after removal of the specimens from their formwork. The samples containing SLC+, however, showed a linear increase in shrinkage over the first 11 days. After this first stage, only small further increases in shrinkage were seen for most samples. The results for samples with SHC+ and SLC+ revealed minor linear expansion. Similarities were seen for the reference between 14 and 28 days and for samples containing PCE1 between 28 and 58 days. The reference specimen reached 98% of the maximum linear shrinkage at ~1 mm/m on day 7. After that, only very small changes were seen over the full course of measurements. On day 7, linear shrinkage of the samples varied between 0.3 and 0.7 mm. While samples with SLC+ reached the smallest value, the samples containing SHC+ reached the greatest.

After 7 days, most of the samples experienced little shrinkage while others showed a slight expansion. This behavior resembles that observed through investigations by Li et al. (2019), who found that expansion took place after the initial autogenous shrinkage of MK-geopolymer. Those authors suggested that the nuclei and gel-formation processes were the cause for that behavior. The expansion was observable within 8 and 42 h of the reaction. In contrast, the expansion of the specimen investigated in the present study (Fig. 7) took place after 7 days. This phenomenon may have other causes, therefore. Thermic expansion can be excluded as a possible cause because of stable environmental conditions during measurements.

After 56 days, most samples reached a linear shrinkage of ~0.7 mm/m, which is 30% less than the value of the reference of ~1.0 mm/m. Samples containing SLC– achieved less linear shrinkage at ~0.53 mm/m, while samples with PCE2 achieved slightly higher values of ~0.78 mm/m.

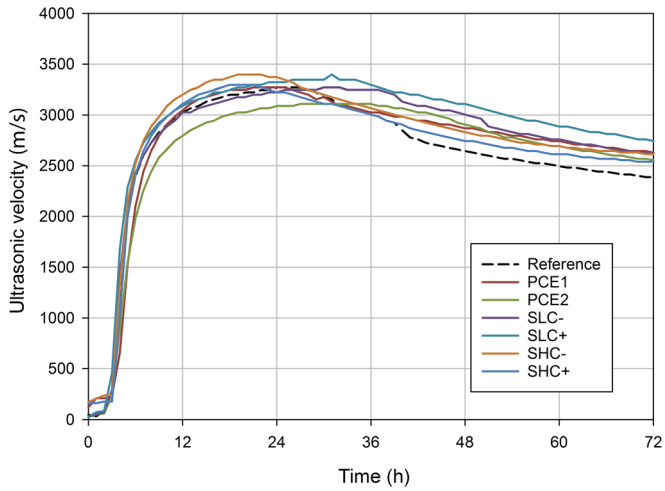

Fig. 5. Ultrasonic velocity over a time period of 72 h

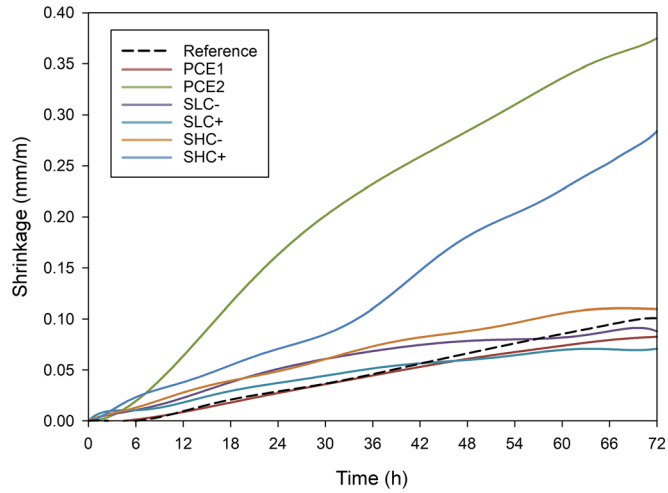

Fig. 6. Linear shrinkage over a period of 72 h

Weight Change

The weight of specimens was recorded simultaneously with the linear-shrinkage measurements. As an example, the data for superplasticizer with a dosage of 0.5 wt.% is displayed (Fig. 8). The recording of weight change started at day 3 when the specimens were removed from the formwork. The reference exhibited a weight loss of ~4.2 wt.% within the first 4–7 days of shrinkage. Equivalent behavior was noticed for samples containing SHC–, while samples including SHC+ demonstrated a further 1 wt.% weight loss. The weight losses of samples incorporating PCE were significantly greater with values of 7 wt.% (PCE1) and 10.3 wt.% (PCE2). Samples containing SLC– and SLC+ showed a considerably smaller weight loss by 0.5 wt.% (SLC+) and 1.1 wt.% (SLC–), and further implied an almost linear weight loss until day 28. After 56 days, the weight losses of these samples and samples containing SHC+ were comparable with the weight loss of the reference specimen which was determined to be 7.0 ± 0.5 wt.%. Weight losses of samples containing SHC– (8.7 wt.%) and PCE2 (9.6 wt.%), and especially PCE1 (11.8 wt.%), were greater.

The quick drying of samples containing PCE2 and the large weight losses of samples containing PCE1 and PCE2 in comparison with the reference are indicators of a larger amount of capillary porosity. These findings are in line with the observations made in the pore analysis, in which samples containing SLC+ and PCE2 showed a distinct reduction or increase in capillary porosity, respectively.

Flexural and Compressive Strength

The results for the flexural strengths of specimens at day 7 revealed only a few deviations from each other (Fig. 9). While the flexural strength of the reference specimen reached a value of ~2.25 N/mm^2, the values of the samples containing PCE1 at high dose or PCE2 at low dose maintained a greater strength at ~3.00 N/mm^2 and 2.85 N/mm^2, respectively. Greater values for samples containing PCE1 at higher dose were obtained

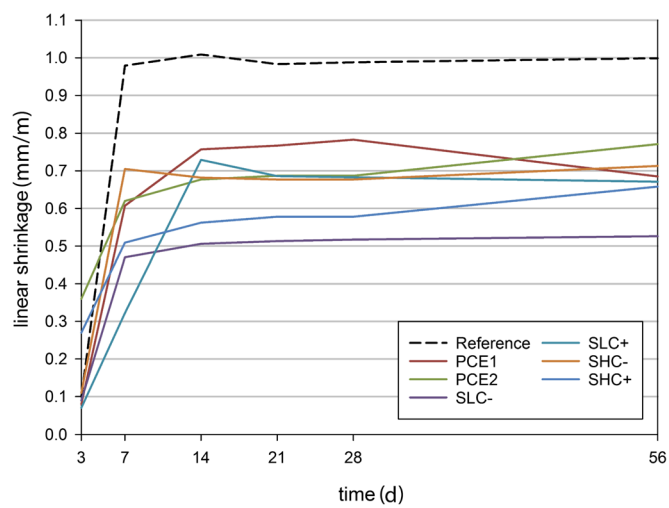

Fig. 7. Linear shrinkage over a period of 56 days

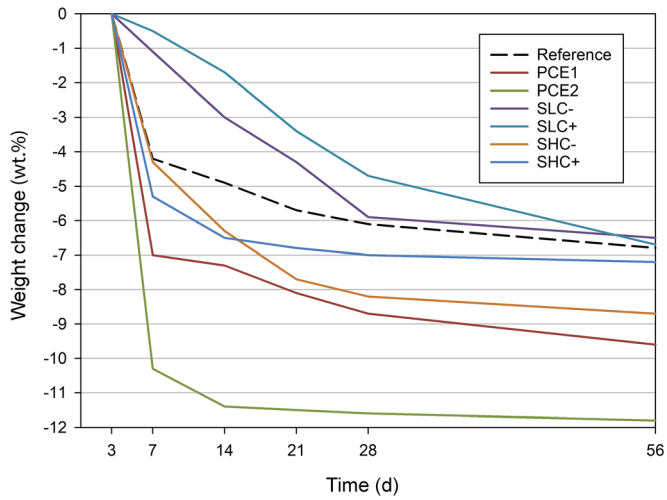

Fig. 8. Weight change of specimens over the course of 56 days

although the samples containing PCE2 had smaller values. All SSP samples reached flexural strengths equal to that of the reference with a trend to increased values for SSPs with greater specific charge density. The greatest flexural strength of all samples containing SSPs was determined for specimens including SHC– with a value of ~2.6 N/mm^2, but a decrease with higher dose.

After 28 days, a clear decline in flexural strength of the reference can be seen (Fig. 10) in comparison to the 7-day flexural strength (Fig. 9). While most samples lack a significant deviation of flexural strength between 7 and 28 days, a clear increase in flexural strength was observed in samples containing larger doses of SLC+ or SLC–. The standard deviations of the samples containing SHC+ or SHC– at higher doses were more than twice as high as the standard deviations of samples with lower doses. Therefore, no coherent dependence of specific charge density and charge polarity can be determined. The flexural strengths of samples incorporating a higher dose of SSPs with low charge density were enhanced after 28 days.

The compressive strengths determined after seven days showed that SSPs tended to improve compressive strength compared to the reference and to samples containing PCE (Fig. 11). The samples containing SHC+ or SHC– achieved the greatest compressive-strength values of ~30 N/mm^2 at low dose. A decrease in compressive strength was observed with increasing dosage for all samples, excluding those containing PCE1. This is particularly evident with samples containing PCE2 or SLC–. The SSPs with large specific charge density led to slightly greater compressive strengths compared to the samples containing SSPs with low specific charge density. The charge polarity of SSPs appeared to have no influence on the compressive strength for high specific charge density. The compressive strength of samples containing SLC– was less significant than of samples containing SLC+.

At a sample age of 28 days, a slight decrease in compressive strength was observed in most samples (Fig. 12) compared to values obtained at day 7 (Fig. 11). An increase in the compressive strength was found for the reference and the samples containing SLC– or PCE2 at higher doses, however.

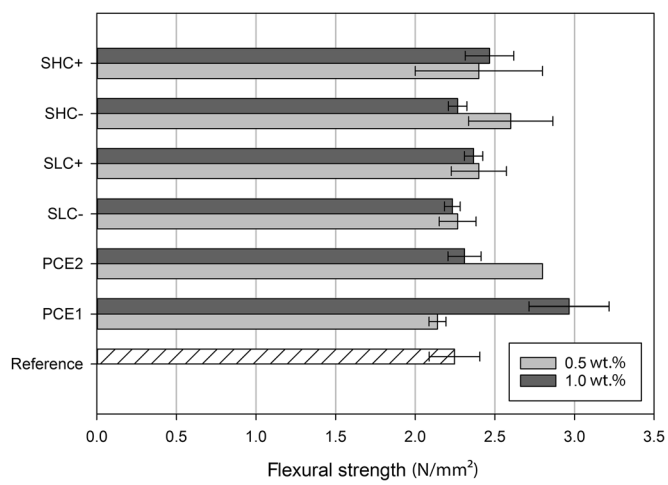

Fig. 9. Flexural strength after 7 days

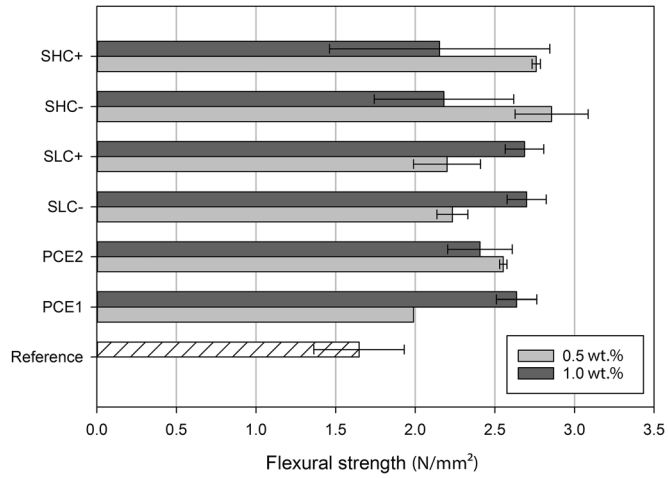

Fig. 10. Flexural strength after 28 days

This was contrary to the significant decrease in compressive strength observed in samples containing a smaller amount of the aforementioned superplasticizers. This behavior cannot be attributed precisely, based on the results available from the present study. The greatest compressive strengths were achieved by samples containing SLC– and SLC+ at high dose as well as SHC– at low dose. The values were similar to the compressive strength of the reference specimens. No trend with respect to the varying charge densities or polarities was found.

Porosity

In terms of durability of concrete and mortar, an excess of capillary pores is unfavorable due to mechanical damage caused by penetrating water while undergoing freeze-thaw cycles and interaction with salts. In the present study, pores with a radius of <0.1 μm were assumed to be gel pores and pores with a radius >0.1 μm were considered to be capillary pores.

The total porosity of detectable pores with 0.003–245 μm radius (apparent porosity) was obtained with 19.9% by volume for the reference (Table 8). The porosity of samples with PCE was determined to be 3–3.5 vol.% greater than that of the reference, while most samples containing SSPs were detected with a 0.7–1.4 vol.% greater porosity. The porosity of the sample incorporating SLC+ was on par with the reference, having a value of 19.3 vol.%. Calculation of the impact of the percentage of gel pores and capillary pores on the measured porosity (Table 8) revealed almost no effect (<1.0%) in samples containing SLC– and SHC–. A small increase in gel pores was found in the sample containing SHC+ (+2.8%) while for the sample with PCE1, a small decrease (–3.4%) was determined. In samples containing PCE2 and SLC+, a significant impact of the superplasticizers on gel pore content was seen, whereby the value of PCE2 was reduced by 11.3% and the value of SLC+ increased by 8.8%. The sample containing SLC+ was positively impacted by having a decreased porosity, while in turn favoring the formation of gel pores over capillary pores.

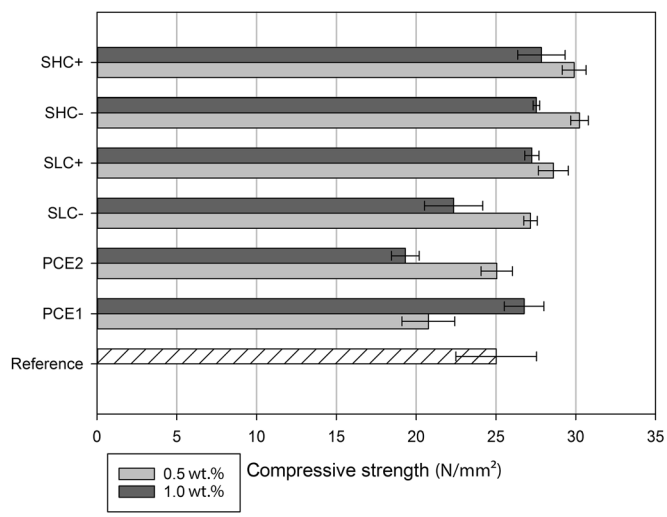

Fig. 11. Compressive strength after 7 days

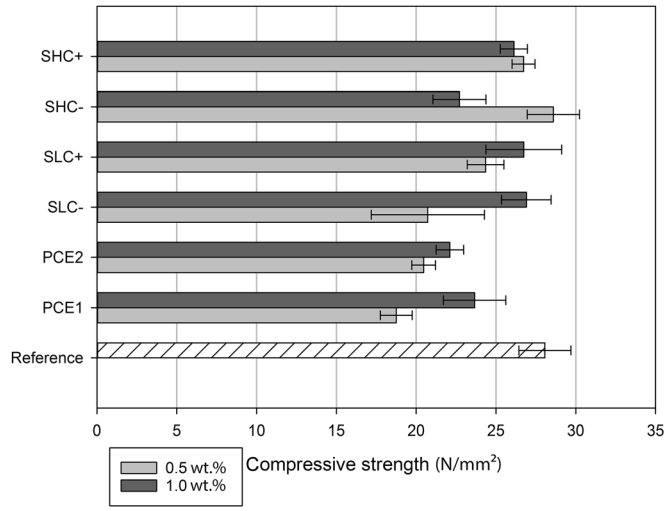

Fig. 12. Compressive strength after 28 days

The cumulative pore-volume distribution (Fig. 13) and the logarithmic differential intrusion volume (Fig. 14) indicated that the large porosity of the sample with PCE2 was accompanied by a strong increase in the number of pores with radii between 0.5 and 2 μm. Within the same range of pore radii, a decrease in porosity compared to the reference was observed in the sample with SLC+, while the values for all other samples increased. The same was seen in the narrow band of radii around 5 μm which appeared as a group of peaks (Fig. 14). While the presence of pores with radii of 0.1 μm or less in samples containing SLC+ and PCE1 was linked to a porosity similar to that of the reference sample, an increase in porosity for samples containing SHC–, SHC+, and PCE2 occurred. The sample containing SLC– represented a completely different pore distribution with a substantial increase in pores with radii of ~0.03 μm.

The addition of SSPs caused a smaller proportion of capillary pores in the range from 1 μm to ~80 μm than was observed in the reference and samples incorporating PCE. The sample with SLC+ was particularly noticeable because of the small number of pores in the range of ~0.5 to 5 μm. A particularly distinct increase in the cumulative pore volume with pore radii <0.02 μm was found. Consequently, this resulted in the lowest detected porosity and the greatest percentage of gel pores (Table 8). The pore size of the sample containing SLC– was enhanced with radii of <0.05 μm. The logarithmic differential intrusion volume distribution (Fig. 14) showed a notable peak at radii of ~0.03 μm.

CONCLUSIONS

In the present study, starch-based superplasticizers (SSPs), which had already been proven to work in cementitious systems, were tested for their effect on metakaolin geopolymer mortar. Four SSPs differing in terms of specific charge density and polarity were synthesized and tested along with two PCEs differing in terms of molecular structure.

The use of SSPs caused an increase in fresh mortar slump of up to 40% at a dosage of 1.0 wt.%, whereas neither PCE had a positive effect on slump. The loss of dispersing ability is a sign of the instability of investigated PCEs ester bonds in very basic media. In contrast, the ether bonds of the SSPs are considered to be stable in such media. The SSPs with positive charge performed slightly better than that with a negative charge.

The air content of fresh mortar samples was reduced slightly with SSPs compared to the reference, while PCEs caused an increase. No impact of superplasticizer dosage (0.5 and 1.0 wt.%) on the air content was seen. PCE are known for their foaming effect and, therefore, are mostly used together with defoaming agents, which could be also unstable in very basic media.

Table 8. Porosity and percentage of gel pores and capillary pores

	Reference	PCE1	PCE2	SLC–	SLC+	SHC–	SHC+
Apparent porosity (vol.%)	19.9	22.9	23.4	21.3	19.3	20.6	20.6
Gel pores (%)	67.6	64.2	56.3	67.9	76.4	68.2	70.4
Capillary pores (%)	32.4	35.8	43.7	32.1	23.6	31.8	29.6

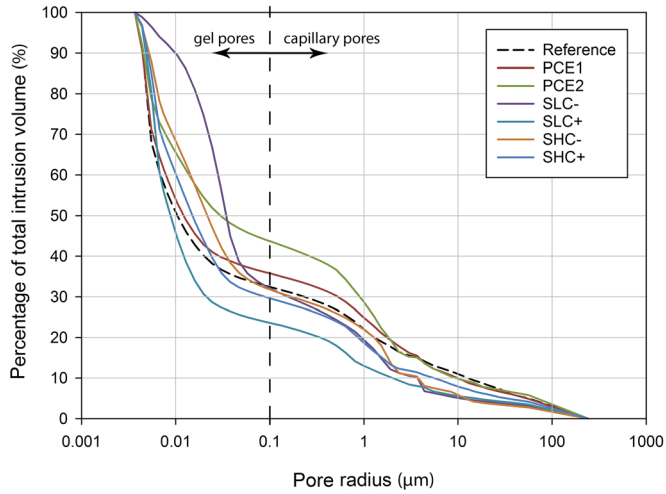

Fig. 13. Cumulative pore-size distribution

Measurement of ultrasonic velocity showed negligible impact of SSPs on the hardening of the MK-geopolymer mortars. A decrease in measured ultrasonic velocity after reaching the maximum values was observed.

The SSPs had a predominantly positive impact on the 7-days compressive strength. After 28 days, the compressive strength of most samples with SSPs was similar to that of the reference, while a significant decrease was seen for samples containing PCE. This is caused by the foaming effect of the PCE, which leads to a greater porosity and, therefore, lower strength compared to the reference. The flexural strength of samples with SSPs was comparable with the reference while the flexural strength of some samples containing PCE, depending on the dosage, increased. After 28 days, a distinct decline in flexural strength of the reference specimen was seen. Analysis of samples containing PCE revealed little or no decline in flexural strength whereas the values for flexural behavior of most samples containing SSPs increased.

With the exception of the sample containing SLC+, porosity in the region of pores with radii between 0.003 and 245 µm was increased for samples containing SSP and even more so for samples containing PCE. The porosity of the sample containing SLC+ was slightly lower than the reference. While SSPs caused a slight increase in gel pores (<0.1 µm) over capillary pores (>0.1 µm), PCEs had the opposite effect. The gel-pore content of samples containing SLC+ increased considerably. This should lead to a greater resistance against permeating media and, therefore, a better durability in comparison to the reference and samples containing PCE.

Further research will be conducted on the interaction of modified starch molecules with metakaolin particles. The investigation of adsorption behavior will include time-dependent zeta-potential measurement and calculation of adsorption rates. For in situ investigations, a UV/Vis-detector coupled with a RI-detector will be used.

The molecular weight distribution of SSPs will be changed by using different base starches as well as adjusting reaction parameters. Size-exclusion chromatography (SEC) will be used to narrow down the molecular weight distribution for better comparison. In addition, the surface tension and foam,

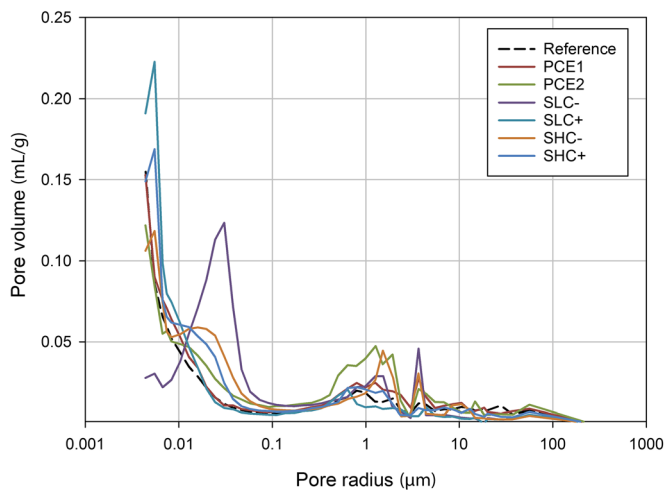

Fig. 14. Logarithmic differential intrusion volume

formation tendency of SSPs as well as the impact on total porosity of the hardened geopolymer will be investigated. The hardened geopolymer structure and fracture formation will be analyzed utilizing environmental scanning electron microscopy and sub-μ computer tomography. Phase formation will be evaluated by means of XRD, FTIR, and nuclear magnetic resonance (NMR) spectroscopy.

ACKNOWLEDGMENTS

The authors thank the Institute of Organic Chemistry and Macromolecular Chemistry of the Friedrich Schiller University Jena for carrying out the GPC analysis.

FUNDING INFORMATION

Open Access funding provided by Projekt DEAL.

Compliance with Ethical Statements

Conflict of Interest

The authors declare that they have no conflict of interest.

REFERENCES

Andrew, R. M. (2018). Global CO_2 emissions from cement production. *Earth System Science Data*, *10*, 195–217. https://doi.org/10.5194/essd-10-195-2018

Bezerra, U. T. (2016). Biopolymers with superplasticizer properties for concrete. In F. Pacheco-Torgal, V. Ivanov, N. Karak, & H. Jonkers (Eds.), *Biopolymers and Biotech Admixtures for Eco-Efficient Construction Materials*. Elsevier, pp. 195–220. https://doi.org/10.1016/B978-0-08-100214-8.00010-5

Crépy, L., Petit, J.-Y., Wirquin, E., Martin, P., & Joly, N. (2014). Synthesis and evaluation of starch-based polymers as potential dispersants in cement pastes and self leveling compounds. *Cement and Concrete Composites*, *45*, 29–38. https://doi.org/10.1016/j.cemconcomp.2013.09.004

Davidovits, J. (2015). *Geopolymer Chemistry and Applications* (4th edition). Saint-Quentin, France: Institut Géopolymère.

Elyamany, H. E., Abd Elmoaty, A. E. M., & Elshaboury, A. M. (2018). Magnesium sulfate resistance of geopolymer mortar. *Construction and Building Materials*, *184*, 111–127. https://doi.org/10.1016/j.conbuildmat.2018.06.212

Favier, A., Hot, J., Habert, G., Roussel, N., & d'Espinose de Lacaillerie, J.-B. (2014). Flow properties of MK-based geopolymer pastes. A comparative study with standard Portland cement pastes. *Soft Matter*, *10*, 1134. https://doi.org/10.1039/c3sm51889b

Fernández-Jiménez, A. & Palomo, A. (2007). Factors affecting early compressive strength of alkali activated fly ash (AAFA) concrete. *Materiales De Construcción*, *57*.

Gay, C. & Raphaël, E. (2001). Comb-like polymers inside nanoscale pores. *Advances in Colloid and Interface Science*, *94*, 229–236. https://doi.org/10.1016/S0001-8686(01)00062-8

Gharzouni, A., Sobrados, I., Joussein, E., Baklouti, S., & Rossignol, S. (2016). Predictive tools to control the structure and the properties of metakaolin based geopolymer materials. *Colloids and Surfaces A: Physicochemical and Engineering Aspects*, *511*, 212–221. https://doi.org/10.1016/j.colsurfa.2016.09.089

Knaus, S. & Bauer-Heim, B. (2003). Synthesis and properties of anionic cellulose ethers: influence of functional groups and molecular weight on flowability of concrete. *Carbohydrate Polymers*, *53*, 383–394. https://doi.org/10.1016/S0144-8617(03)00106-1

Koenig, A., Herrmann, A., Overmann, S., & Dehn, F. (2017). Resistance of alkali-activated binders to organic acid attack: Assessment of evaluation criteria and damage mechanisms. *Construction and Building Materials*, *151*, 405–413. https://doi.org/10.1016/j.conbuildmat.2017.06.117

Kuenzel, C., Grover, L. M., Vandeperre, L., Boccaccini, A. R., & Cheeseman, C. R. (2013). Production of nepheline/quartz ceramics from geopolymer mortars. *Journal of the European Ceramic Society*, *33*, 251–258. https://doi.org/10.1016/j.jeurceramsoc.2012.08.022

Le Quéré, C., Andrew, R. M., Friedlingstein, P., Sitch, S., Hauck, J., Pongratz, J., et al. (2018). Global Carbon Budget 2018. *Earth System Science Data*, *10*, 2141–2194. https://doi.org/10.5194/essd-10-2141-2018

Lei, L. & Plank, J. (2012). A concept for a polycarboxylate superplasticizer possessing enhanced clay tolerance. *Cement and Concrete Research*, *42*, 1299–1306. https://doi.org/10.1016/j.cemconres.2012.07.001

Lei, L. & Plank, J. (2014). A study on the impact of different clay minerals on the dispersing force of conventional and modified vinyl ether based polycarboxylate superplasticizers. *Cement and Concrete Research*, *60*, 1–10. https://doi.org/10.1016/j.cemconres.2014.02.009

Li, Z., Zhang, S., Zuo, Y., Chen, W., & Ye, G. (2019). Chemical deformation of metakaolin based geopolymer. *Cement and Concrete Research*, *120*, 108–118. https://doi.org/10.1016/j.cemconres.2019.03.017

Lizcano, M., Gonzalez, A., Basu, S., Lozano, K., & Radovic, M. (2012). Effects of water content and chemical composition on structural properties of alkaline activated metakaolin-based geopolymers. *Journal of the American Ceramic Society*, *95*, 2169–2177. https://doi.org/10.1111/j.1551-2916.2012.05184.x

Lv, S. H. (2016). High-performance superplasticizer based on chitosan. In F. Pacheco-Torgal, V. Ivanov, N. Karak, & H. Jonkers (Eds.), *Biopolymers and Biotech Admixtures for Eco-Efficient Construction Materials*. Elsevier, pp. 131–150. https://doi.org/10.1016/B978-0-08-100214-8.00007-5

Ng, S. & Plank, J. (2012). Interaction mechanisms between Na montmorillonite clay and MPEG-based polycarboxylate superplasticizers. *Cement and Concrete Research*, *42*, 847–854. https://doi.org/10.1016/j.cemconres.2012.03.005

Palacios, M. & Puertas, F. (2004). Stability of superplasticizer and shrinkage-reducing admixtures in high basic media. *Materiales De Construcción*, *54*.

Partschefeld, S. & Osburg, A. (2018a). Bio-based superplasticizers for cement-based materials. In M. M. R. Taha (Ed.), *International Congress on Polymers in Concrete (ICPIC 2018)* (Vol. 45, pp. 77–82). Cham: Springer International Publishing. https://doi.org/10.1007/978-3-319-78175-4_7

Partschefeld, S. & Osburg, A. (2018b). Untersuchungen zum Einfluss von Stärke-basierten Fließmitteln auf die frühe

Hydratation von Portlandzement von Portlandzement. In H.-M. Ludwig (Ed.), *Proceedings of the 20th Internationale Baustofftagung (ibausil), 12–14. September 2018, Weimar: Internationale Baustofftagung, 12-14 September 2018, Weimar, Bundesrepublik Deutschland*. Weimar: F.A. Finger-Institut für Baustoffkunde, Bauhaus-Universität.

Plank, J., Sakai, E., Miao, C. W., Yu, C., & Hong, J. X. (2015). Chemical admixtures — Chemistry, applications and their impact on concrete microstructure and durability. *Cement and Concrete Research*, *78*, 81–99. https://doi.org/10.1016/j.cemconres.2015.05.016

Pouhet, R., Cyr, M., & Bucher, R. (2019). Influence of the initial water content in flash calcined metakaolin-based geopolymer. *Construction and Building Materials*, *201*, 421–429. https://doi.org/10.1016/j.conbuildmat.2018.12.201

Reganold, J. P. & Harsh, J. B. (1985). Expressing cation exchange capacity in milliequivalentsper 100 grams and in SI units. *Journal of Agronomic Education*, *14*, 84–90.

Saxena, S. K., Kumar, M., & Singh, N. B. (2017). Fire Resistant Properties of Alumino Silicate Geopolymer cement Mortars. *Materials Today: Proceedings*, *4*, 5605–5612. https://doi.org/10.1016/j.matpr.2017.06.018

Sowoidnich, T. (2015). *A study of retarding effects on cement and tricalcium silicate hydration induced by superplasticizers*. Retrieved from https://e-pub.uni-weimar.de/opus4/frontdoor/index/index/docId/2544

Turner, L. K. & Collins, F. G. (2013). Carbon dioxide equivalent (CO_2-e) emissions: A comparison between geopolymer and OPC cement concrete. *Construction and Building Materials*, *43*, 125–130. https://doi.org/10.1016/j.conbuildmat.2013.01.023

(Received 29 September 2019; revised 10 June 2020; AE: Georgios D. Chryssikos)